Hindawi
Journal of Nanomaterials
Volume 2020, Article ID 3136078, 13 pages
https://doi.org/10.1155/2020/3136078

Research Article

Cavitation-Enhanced Delivery of the Nanomaterial Graphene Oxide-Doxorubicin to Hepatic Tumors in Nude Mice Using 20 kHz Low-Frequency Ultrasound and Microbubbles

Zhi Yong Shen,[1] **Bei Qi Shen**,[2] **Ai Jun Shen**,[1] **and Xin Hua Zhu**[3]

[1]*Department of Radiology, Affiliated Tumor Hospital of Nantong University, 226361, China*
[2]*Class 1808, College of Chemical Engineering, Graduate School of Beijing University of Chemical Technology, 100029, China*
[3]*Department of Pathology, Affiliated Tumor Hospital of Nantong University, 226361, China*

Correspondence should be addressed to Zhi Yong Shen; ntszy1426@126.com

Received 12 March 2020; Revised 14 May 2020; Accepted 3 June 2020; Published 29 June 2020

Academic Editor: Zehra Durmus

Graphene oxide (GO) is a kind of nanomaterial. Here, we explored its application in tumor treatment. We loaded doxorubicin onto the surface of GO to form graphene oxide-doxorubicin (GO-DOX). After injection of the contrast agent SonoVue microbubbles (MBs) into the tail vein of tumor-bearing nude mice, subcutaneous hepatic carcinomas inoculated with the HepG2 cell line were irradiated with 20 kHz low-frequency ultrasound (US). Subsequently, GO-DOX was injected into the tail vein of nude mice. Transmission electron microscopy (TEM) and TUNEL assays were performed to observe the curative effects. Biocompatibility tests of GO-DOX included routine blood cell counts, blood smears, serum biochemical assays, and histological sampling of important organs. It was found that the nanomaterial GO-DOX promoted apoptosis of tumor cells in nude mice. TEM of the USMB+GO-DOX treatment showed vascular endothelial cell wall rupture, widened endothelial cell gaps, black granules in the vascular lumen, interstitial erythrocyte leakage, and apparent apoptosis of tumor cells. There were no toxic side effects of GO-DOX on the blood system and in the major organs of these mice. Ultrasound cavitation destroys tumor blood vessels and enhances the release of nanomaterials to tumor cells of nude mice.

1. Introduction

Chemotherapy is one of the main methods of clinically treating malignant tumors, especially advanced-stage tumors [1]. Anthracycline antibiotics [2] are a type of chemotherapeutic drug that have been studied and developed rapidly in the past 30 years. Doxorubicin (DOX) is one of the most commonly used and important anthracycline antibiotics [3]. DOX is a broad-spectrum antineoplastic drug that can produce a wide range of biochemical effects on the body and has a strong cytotoxic effect [4]. Mechanistically, DOX intercalates with DNA [5] to inhibit nucleic acid synthesis [6] and is used in the treatment of cancers, such as acute leukemia [7], breast [8], lung [9], and liver cancers [10]. However, after systemic intravenous injections, toxic reactions resulting from DOX administration are inevitable and include granulocytopenia and thrombocytopenia [11]; hair loss of differing degrees [12]; cardiac toxic symptoms [13], such as arrhythmia, ventricular block, and heart failure [14]; digestive tract symptoms, such as nausea, vomiting, and loss of appetite [15]; and tissue ulcers and necrosis [16].

However, if DOX is combined with nanomaterials, the toxic side effects of systemic blood circulation *in vivo* can be greatly reduced [17]. Graphene is a new nanomaterial with a two-dimensional honeycomb structure and is the thinnest nanomaterial discovered thus far [18]. It has excellent mechanical, thermal, electrical, and optical properties [19] and has potential widespread applications in biomedicine [20], biosensors, and electrochemistry [21]. In recent years, many researchers have explored the application of graphene in biomedicine, especially in biological targeting and drug delivery [22]. Graphene has a large specific surface area [23] and can be loaded with drugs on its upper and lower surfaces and its edges [24]. The loading capacity of graphene is

much higher than that of other nanomaterials [25]. When graphene is oxidized to graphene oxide (GO), the carboxyl, hydroxyl, and epoxy groups are added to the structure [26], which improves its water solubility [27] and makes it easier to dissolve *in vivo* and move into blood circulation [28].

The anthracene ring of DOX and the benzene ring of GO can be strongly linked by π-π conjugation [29]. The hydroxyl and amino groups of DOX can form hydrogen bonds with the hydroxyl and carboxyl groups of GO [29] and can be thus firmly connected, having good loading effects. Under tumoral acidic conditions, the release of the nanomaterial graphene oxide-doxorubicin (GO-DOX) increases [30, 31]. However, tumors have barriers, such as the tumor endothelial barrier and the vascular barrier [32]. How to break down or disrupt the tumor endothelial barrier [33], increasing tumor blood perfusion and permeability [34], in order to increase the local absorption of drugs, is an extensively discussed topic and is still a difficult unresolved problem.

One characteristic of low-frequency (20-100 kHz [35]) ultrasound (US) is the cavitation effect [36]. The cavitation effect refers to the periodic oscillation of microbubbles (MBs) under the action of the US field [37]. Cavitation effects can be divided into stable cavitation and transient cavitation [38]. Stable cavitation refers to the symmetrical compression and expansion of MBs under low acoustic pressure, and the bubble diameter remains relatively constant without breaking down [39]. Transient cavitation refers to the asymmetrical compression and expansion of MBs under higher acoustic pressure which eventually break down and produce a series of physical and chemical effects, such as the destruction of biological cell membranes, an increase in cell membrane permeability [40, 41], the acceleration of chemical syntheses [42], and the production of sonoluminescence [43]. Previous studies have disclosed that 20 kHz low-frequency US irradiation of MBs leads to the rupturing of tumor blood vessels [44]. Subsequently, the endothelial cell gap widens, the capillary permeability increases, and the vascular barrier is destroyed [45].

However, ultrasonic cavitation combined with the GO has not been reported. Thus, in this research, low-frequency US combined with MBs (USMB) was used to irradiate transplanted subcutaneous hepatocellular carcinoma tumors in nude mice to destroy the blood vessels of these tumors and increase drug permeability. Then, GO-DOX was injected into the tail vein of nude mice. The aim of this study was to observe the effect of USMB combined with GO-DOX on hepatocellular carcinomas in nude mice.

2. Materials and Methods

2.1. Materials and Chemotherapy Drugs. Graphite sheets were purchased from Shanghai Yifan Graphite Co., Ltd. (Shanghai, China). H_2SO_4 (98%), H_2O_2 (30% by weight), $NaNO_3$, HCl, Na_2SO_4, $KMnO_4$, and deionized water were obtained from Shanghai Yuanji Chemical Co., Ltd. (Shanghai, China). DOX was purchased from Shanghai Demo Pharmaceutical Technology (Shanghai, China). The chemotherapeutic drug used was GO-DOX. GO was prepared using the Hummer method [46]. Briefly, graphite (0.5 g), $NaNO_3$ (0.5 g), and 23 mL of concentrated H_2SO_4 were mixed and stirred in an ice bath for 1 hour, followed by the slow addition of 1.5 g $KMnO_4$ into the solution with stirring at 35°C for 1 day. Next, 23 mL of deionized water was slowly added to prevent the reaction temperature from exceeding 98°C and was stirred for 30 minutes. Finally, 5 mL of H_2O_2 and 70 mL of deionized water were added. The reaction mixture was filtered by gravity filtration, and the product was washed with HCl (3%) and deionized water consecutively. These processes were repeated several times along with centrifugation. The freeze-drying method was used to prevent GO aggregation.

2.2. Construction of GO-DOX. DOX was dissolved in phosphate-buffered saline (PBS) (pH 8) containing 40 μg/mL GO under 280 W of US treatment for 0.5 hours. Then, the reaction was maintained at 23°C, in the dark, for 24 hours with gentle magnetic stirring. The resulting product was purified by dialyzing (MWCO 8000-10,000 Daltons) against deionized water. The DOX loading in GO was confirmed by measuring the absorbance (300-700 nm) of GO and GO-DOX, respectively, using a microplate reader (Synergy H1; BioTek, Winooski, VT, USA) [47].

2.3. Drug Loading Efficiency. Using a series of different amounts of DOX dissolved in a GO solution of 40 μg/mL, an ultrasonic wave was used for 1 h and shaken on an oscillator in the dark for 12 h. Then, the solution was centrifuged at 14,000 rpm for 1 h. The supernatant was taken and measured at 485 nm by UV-Vis spectrophotometry. The loading efficiency was calculated as $(M_{\text{total}} - M_{\text{upper layer}})/M_{\text{GO}} \times 100\%$, which was 40 μg ÷ 40 μg × 100% = 100%.

2.4. Characterization of GO-DOX. Field emission scanning electron microscopy (FE-SEM) images were taken on an S-4800 (Hitachi Co., Japan) at an accelerating voltage of 15 kV after coating gold on the samples. The field emission transmission electron microscopy (FE-TEM) images were captured using a Tecnai G2 F30 S-TWIN (FEI Co., USA) operating at 200 kV.

2.5. Animal Protocols. All nude mice were aged 5 to 6 weeks, weighed 20 to 22 g, and were purchased from Shanghai Slack Experimental Animal Co., Ltd. (production license (Shanghai 2017-0005)). They were kept in specified pathogen-free (SPF) animal rooms at the Nantong University Animal Experiment Center (use license (Su 2017-0046)) and provided sterilized water and chow *ad libitum*. Animal feeding and treatments were approved by the animal ethics committee of the Animal Center of Nantong University. During the experiments, humane care was given to the laboratory animals according to the 3R principle (reduction, replacement, and refinement).

2.6. Subcutaneous Tumor Model. Following the administration of anesthesia by intraperitoneal injection of 70 mg/kg of sodium pentobarbital, the mice were secured to a sterile bench according to the principles of aseptic operation. Each mouse was then subcutaneously inoculated with 1×10^7 HepG2 cells into the flank after local sterilization. The mice

remained in SPF conditions after the operations and were observed at 3-day intervals. Two weeks later, the experiments were initiated when the tumors had reached a size of 6 to 7 mm.

2.7. Ultrasound Instruments and Microbubbles (MBs). The ultrasonic therapeutic apparatus (Jiangsu Han Mei Biotechnology, Taizhou, China) has a transmitting frequency of 20 kHz, a sound intensity of 2 W/cm^2, and a duty cycle of 40% (on 2 s, off 3 s). The diameter of the ultrasonic probe is 2 cm. The wavelength of the ultrasonic wave that 20 kHz ultrasound produced is 7 cm, with the amplitude 60 μm.

We used pulse waves with the duty cycle of 40% for the following reasons. First, it was reported that continuous wave ultrasound observations have theoretically emphasized thermal bioeffects, whereas the pulsed ultrasound observations have emphasized cavitation [48]. Second, the method of on 2 s and off 3 s is easy to operate and control manually. Third, the intermittent time of 3 s makes the bubbles have enough time to enter the tumor blood vessels again through the blood circulation of nude mice and continue to produce cavitation biological effect.

The MBs used were an US contrasting agent (SonoVue; Bracco SpA, Milan, Italy), and the bubble suspension consisted of 59 mg sulfur hexafluoride and 5 mL of saline. The concentration of the contrasting agent was 1.8×10^9 MBs/mL. The average diameter of the MBs was approximately 2.5 μm; the 90% microbubble diameter was less than 6 μm.

Cavitation depends on the vibration of microbubbles (cavitation nuclei) in the sound field. Due to the lack of cavitation nuclei in normal animals, we injected MBs into nude mice from the tail vein. This can not only significantly increase the number of cavitation nuclei enhancing the cavitation effect of low-frequency ultrasound but also greatly reduce the cavitation threshold [49].

The cavitation effect is related to the initial radius of bubbles, the number of bubbles, and the frequency of ultrasonic wave. As the initial radius of bubbles increases, the natural frequency of bubbles decreases [50]. With the increase of bubble number density, the natural resonance frequency of bubble decreases [50]. This is mainly because, in the bubble cloud system, the coupling oscillation between bubbles increases the constraint of the system on each bubble; the signal bubble is suppressed, so the resonant frequency of the bubble is reduced. For example, it is reported that if the number of bubbles is 5000, the free vibration frequency of bubbles with an initial radius of 5 μm in the group is about 143 kHz [50]. The lower the ultrasonic frequency is, the longer the vibration period of bubbles and more time of expansion phase they have [45]. In the compression phase, when bubbles collapse, a stronger cavitation effect is produced [45]. It is reported that driving frequencies in the low-frequency range (i.e., 20 kHz) are associated with larger and violently collapsing bubbles while driving frequencies in the MHz range are associated with a shorter life cycle of smaller cavitation bubbles [37]. 20 kHz ultrasonic has been widely researched theoretically [51] and used in industry. Ultrasound (20 kHz) could improve the physicochemical properties of beef myofibrillar proteins [52]. US at a frequency of 20 kHz has been used to degrade the antibiotic ofloxacin in water [53]. Low-frequency (20 kHz) ultrasound could be applied for heavy metal decontamination of milk without affecting its physical, chemical, and microbiological properties [54].

The 20 kHz ultrasound has also been applied in medicine. Low-frequency ultrasound (20 kHz) enhances myocardial contractility [36]. Husseini et al. demonstrated that lower ultrasound frequencies (20 kHz) achieved the higher levels of release of the anticancer agent DOX, compared with the efficiency of drug release decreased with increasing frequency up to 90 kHz [55].

The use of low-frequency (20 kHz) and low-energy (3.77 W/cm^2, 10% duty cycle) ultrasound in combination with bubbles (SonoVue) could be a promising physical method of increasing drug/gene delivery efficiency [56]. The dose of MBs injected into the tail vein of the mice was 0.2 mL for each treatment. The injection rate is 0.05 mL/s. The probe was placed on the subcutaneous tumors of the mice, with an ultrasound transmission gel (a lotus medical ultrasonic coupling agent, Yijie Guangzhou Pharmaceutical Technology Co., Ltd., China) being interposed to ensure US propagation. The sonication time was 1 minute, once every other day, for 2 weeks.

2.8. Groups. Forty tumor-bearing nude mice were randomly divided into four groups, with 10 mice in each group. The A group was the negative control group (sham treatment). The B group (USMB group) had 0.2 mL of MBs injected into the tail vein; the tumor was simultaneously irradiated with 20 kHz US for 1 minute, once every other day, for 2 weeks (Figure 1). Compared to our previous 26 mW/cm^2 for 3-minute irradiation, the energy of the 2 W/cm^2 was too large, and the skin of nude mice would be significantly damaged and burned by ultrasound exposure for 3 minutes. Therefore, we shortened the irradiation time to 1 minute to ensure the therapeutic effect on tumors and protect the skin of nude mice. The C group (GO-DOX group) had a drug loading efficiency of 100%, with a GO concentration of 40 μg/mL and a DOX concentration of 40 μg/mL. The injected drug concentration for each mouse at each time was as follows: DOX, 40 μg/mL, 0.3 mL, or 12 μg or 0.6 mg/kg; GO, 40 μg/mL, 0.3 mL, or 12 μg or 0.6 mg/kg, and it was injected into the tail vein of nude mice at a speed of 0.06 mL/s. The drug was injected once every other day for 2 weeks (Figure 2). The D group (USMB+GO-DOX group) received 2 weeks of USMB followed by 2 weeks of GO-DOX.

At the end of the therapy experiments, 20 mice, made up of 5 random mice from each group, were euthanized. The cancers were collected and cut into two sections for cell apoptosis detection and transmission electron microscopy. Biocompatibility tests of GO-DOX were performed, including routine blood cell counts, blood smears, serum biochemical assays, and histological sectioning of the major organs. The remaining 20 mice, 5 from each group, were housed and fed continuously, and the overall survival time was calculated.

2.9. Cell Apoptotic Detection. Apoptotic cells were visualized by 5′-deoxyuridine triphosphate biotin nick end labeling

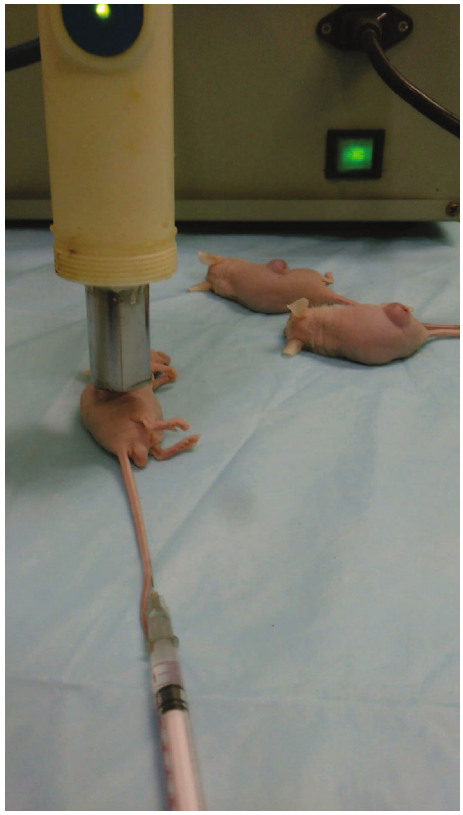

Figure 1: Tumor irradiation by US immediately after injection of microbubbles into the tail veins.

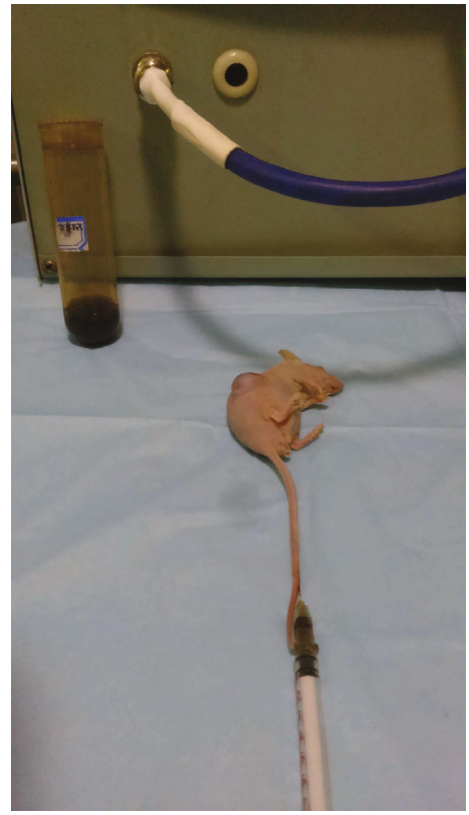

Figure 2: Tumors treated by GO-DOX injected into the tail vein.

(TUNEL). The TUNEL kit (POD) was purchased from Roche Molecular Biochemicals (Basel, Switzerland). The assay was performed per the manufacturer's instructions and other references [57]. Samples were considered TUNEL-positive when the nucleolus appeared as an obvious brown granule. Ten high-powered fields (200x) were observed on each slide, and at least 1000 positive cells were scored at random. The apoptotic index (AI, percentage of TUNEL-positive cells) was calculated as the number of TUNEL-positive cells ÷ the total number of cancer cells × 100%.

2.10. Transmission Electron Microscopy (TEM) of Tumor Tissues. Each tumor sample, ~1 mm^3, for TEM was fixed in 2% glutaraldehyde in PBS for 2 hours at 4°C, followed by two washes in PBS each for 10 minutes. After treatment with 1% osmium tetroxide in PBS, specimens were fixed at 4°C for 2 hours and dehydrated with 30%, followed by 50%, followed by 70% ethanol three times each for 10 minutes. The samples were then embedded in propylene oxide for 2 hours and stained with lead citrate. Finally, after sectioning, the specimens were examined by TEM (Philips CM-120; Philips, Eindhoven, The Netherlands).

2.11. Biocompatibility Detection of GO-DOX. GO is toxic for the liver, spleen, lung, intestine, and brain, but not the heart [58]. The toxic effects are dose-dependent. *In vivo* applications of high doses (10 mg/kg body weight of mice for 14 days) of GO may result in toxic effects, such as inflammatory cell infiltration, pulmonary edema, and granuloma formation [59]. GO can also induce neurotoxic effects in rats. For example, intraperitoneal injection of GO in male BALB/c mice at a dose of 4 mg/kg for seven consecutive days caused brain damage [60]. GO can also cause mitochondrial damage, including a decrease in mitochondrial membrane potential, reduction of ATP production, dysregulation of Ca^{2+} homeostasis, interference with the electron transport chain by disturbing electron transfer, and overproduction of reactive oxygen species [61]. Due to the above mentioned side effects of GO, the biocompatibility detection of GO-DOX in nude mice is necessary.

The toxic tests of GO-DOX include blood cell counts, blood smears, serum biochemical assays, and histological sectioning of important organs.

To obtain a small amount of blood from the mouse, a cut from the tip of the tail vein of the mouse is sufficient. However, if large amounts of blood are needed, retroorbital bleeding of the mice is performed [62]. After eyeball extraction of the mice, ethylenediaminetetraacetic acid- (EDTA-) K2 anticoagulant was added, and the blood specimens were sent for examination. For blood cell counts, the levels of serum red blood cells (RBC), hemoglobin (HB), platelets (PLT), and white blood cells (WBC) were measured on a Sysmex XS-800i automatic blood routine detector (Hieson Meikang Company, Tokyo, Japan). Blood smears were evaluated using Wright staining. In the serum biochemical assays, the levels of serum alanine aminotransferase (ALT), aspartate aminotransferase (AST), creatinine (CREA), and blood urea nitrogen (BUN) were measured on a Hitachi 7600-210 automatic biochemical analyzer (Hitachi High-Technologies, Tokyo,

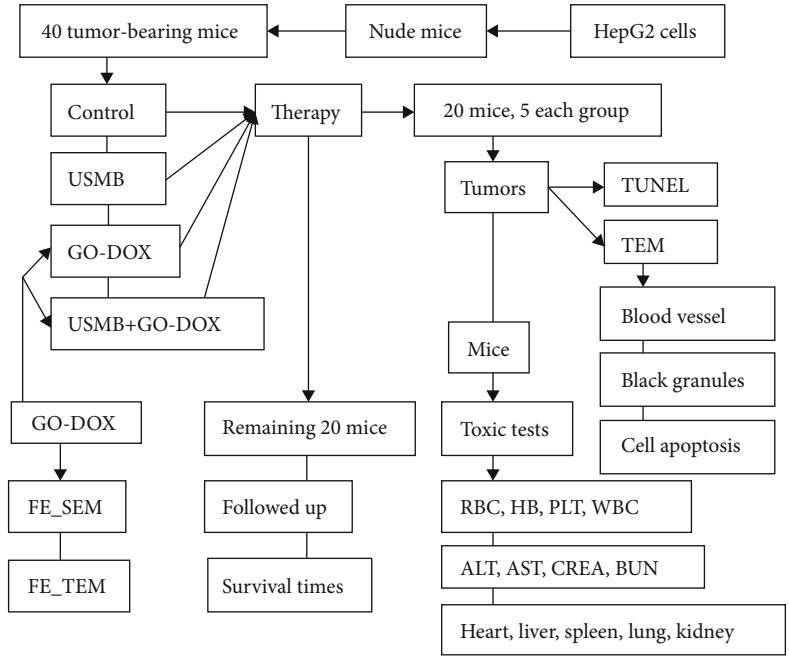

Figure 3: Experimental scheme design (USMB: low-frequency ultrasound combined with microbubbles; GO-DOX: graphene oxide-doxorubicin; FE-SEM: field emission scanning electron microscopy; FE-TEM: field emission transmission electron microscopy; TEM: transmission electron microscopy; RBC: red blood cells; HB: hemoglobin; PLT: platelets; WBC: white blood cells; ALT: alanine aminotransferase; AST: aspartate aminotransferase; CREA: creatinine; BUN: urea nitrogen).

Japan). In the major organ examinations, histological sections of the heart, liver, spleen, lung, and kidney were examined using hematoxylin and eosin (HE) staining.

2.12. Survival Time Follow-Up. The survival time was calculated based on the date of tumor incubation and the date of death. At the end of the experiment, the survival times of the 20 treated nude mice in each group of euthanized mice were calculated using a right censoring survival model. The survival times of the remaining 20 nude mice in each group were followed up. The survival curves were calculated using the Kaplan–Meier method and were analyzed using the log-rank test.

Schematic of the experimental arrangement is in Figure 3.

2.13. Statistical Analyses. The results are expressed as the mean ± standard deviation (SD). The data were analyzed using Student's t-test. Survival curves were calculated using the Kaplan–Meier method and were analyzed using the log-rank test. Values of $P < 0.05$ are considered significant.

3. Results

3.1. FE-SEM and FE-TEM of GO-DOX. The results of the preparation of GO-DOX are illustrated in Figures 4 and 5. The FE-SEM analysis of GO-DOX is shown in Figure 4. It presented a smooth surface, appearing silk-like in structure. As seen in Figure 5, FE-TEM shows that GO has a very thin and transparent film structure providing a good platform for DOX to load onto its upper and lower surfaces and its edges, thus confirming its role as a nanodrug carrier.

3.2. Tumor Cell Apoptotic Rate. The average apoptotic rates of tumor cells in the control, USMB, GO-DOX, and USMB +GO-DOX groups were 8.2 ± 3.49%, 40 ± 9.51%, 48.6 ± 8.96%, and 62.4 ± 7.27%, respectively. There was a significant difference between the USMB+GO-DOX and the control, USMB, and GO-DOX groups with $t = 15.03$, $P < 0.0001$; $t = 4.18$, $P = 0.0031$; and $t = 2.67$, $P = 0.0282$, respectively (Figures 6 and 7).

3.3. TEM of Tumor Tissue in the Four Groups. TEM of tumor tissues demonstrated that in the control group, the vascular endothelium was intact and the vascular wall was unbroken. Furthermore, RBC were seen in the vascular lumen, there were no black granules, and tumor cell apoptosis was rare. In contrast, the USMB-treated group presented with incomplete vascular endothelium, blood vessel wall rupture, erythrocyte hemorrhage outside the lumen, no black granules in the vascular lumen, and apoptosis of tumor cells. In the GO-DOX group, the vascular endothelium was intact without vessel wall rupture, RBC were located in the vessel lumen, black granules were seen in the vascular lumen, and tumor cell apoptosis was found. In the USMB+GO-DOX group, the vascular endothelium was incomplete with broken blood vessel walls, RBC leaked from the blood vessels into the tumor tissue interstitium, black granules were found in the vascular lumen, and apoptosis of tumor cells was obvious (Table 1, Figure 8).

3.4. Toxicity of GO-DOX Biocompatibility Detection

3.4.1. Blood Cell Counts and Blood Smears. The results of the blood tests with RBC, HB, PLT, and WBC counts are provided in Table 2. There were no significant differences

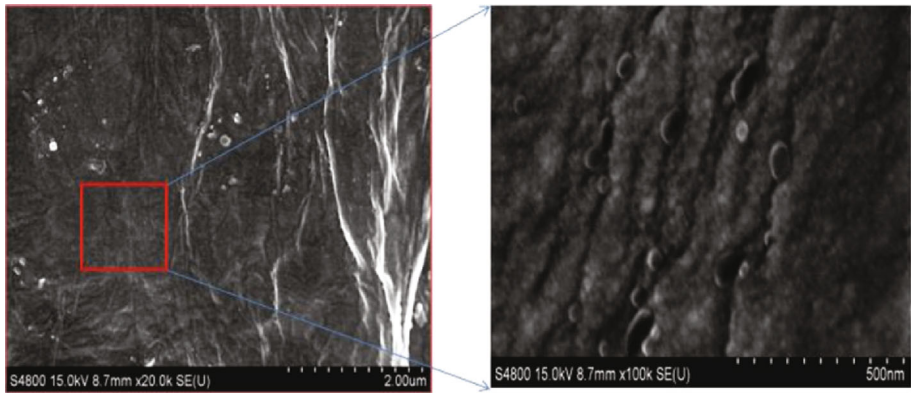

Figure 4: FE-SEM images of GO-DOX.

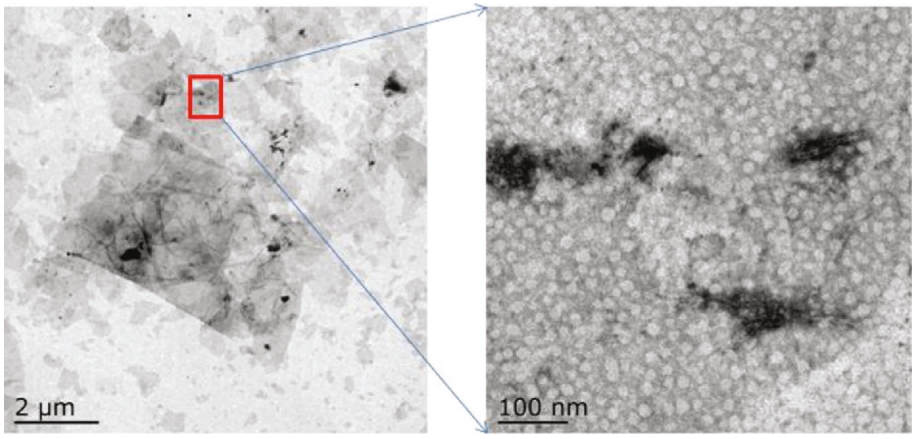

Figure 5: FE-TEM images of GO-DOX.

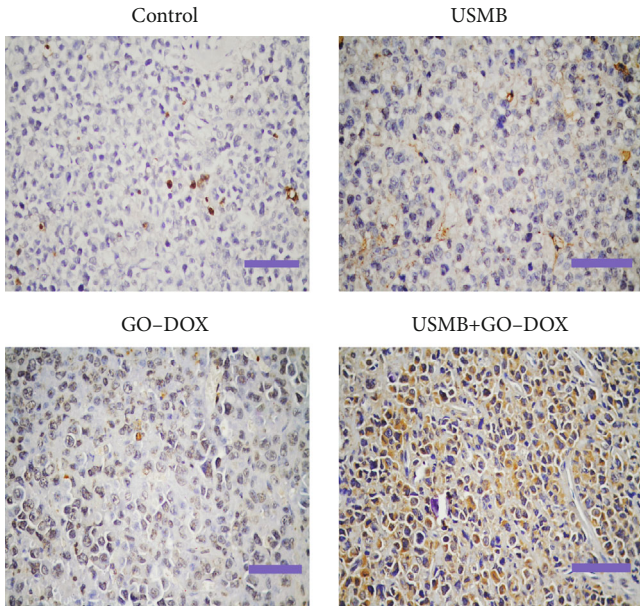

Figure 6: TUNEL results of tumor cell apoptosis (200x; bar: 50 μm).

between the USMB+GO-DOX and the control, USMB, and GO-DOX groups in RBC counts, with $t = 0.18$, $P = 0.8586$; $t = 0.36$, $P = 0.7257$; and $t = 0.2$, $P = 0.8458$, respectively.

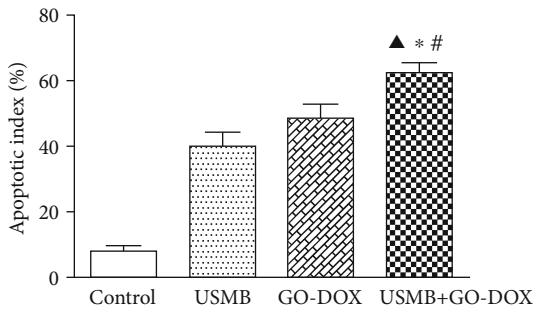

Figure 7: Apoptotic index of the treated groups (▲: vs. control, $P < 0.05$; ∗: vs. USMB, $P < 0.05$; #: vs. GO-DOX, $P < 0.05$).

There were no significant differences between the USMB +GO-DOX and the control, USMB, and GO-DOX groups in HB counts, with $t = 0.57$, $P = 0.585$; $t = 0.38$, $P = 0.7167$; and $t = 0.41$, $P = 0.687$, respectively. There were no significant differences between the USMB+GO-DOX and the control, USMB, and GO-DOX groups in PLT counts, with $t = 0.05$, $P = 0.9617$; $t = 0.52$, $P = 0.617$; and $t = 0.09$, $P = 0.9319$, respectively. There were no significant differences between the USMB+GO-DOX and the control, USMB, and GO-DOX groups in WBC counts, with $t = 1.75$, $P = 0.1181$; $t = 1.32$, $P = 0.2237$; and $t = 0.64$, $P = 0.5388$, respectively.

Table 1: TEM of the vasculation in tumor tissues of nude mice in the four groups.

	Integrity of vascular endothelial cells	Vascular wall rupture	Extravascular erythrocyte	Black particles	Apoptosis of tumor cells
Control	Yes	No	No	No	Few
USMB	No	Yes	Yes	No	Some
GO-DOX	Yes	No	No	Yes	Some
USMB+GO-DOX	No	Yes	Yes	Yes	More

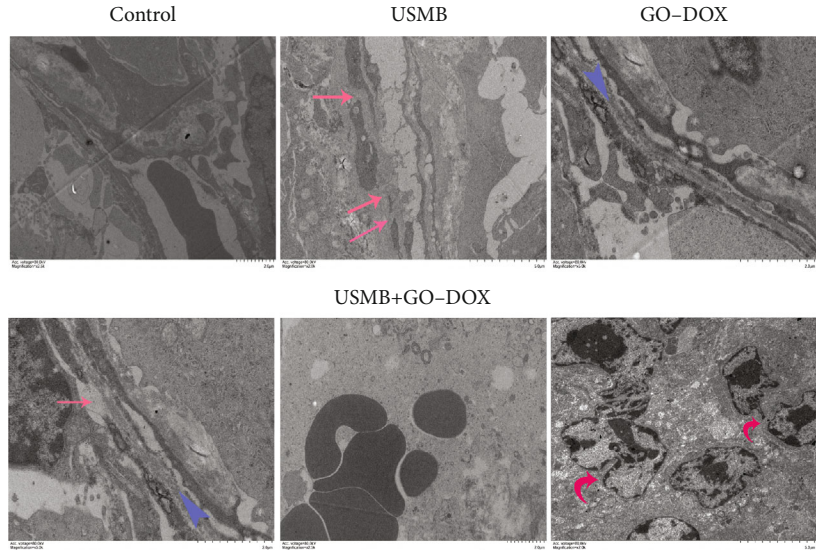

Figure 8: TEM of blood vessels and tumor cells (red arrow: blood vessel rupture area; blue arrow: GO-DOX sheet; red curved arrow: cell apoptosis).

Table 2: Blood cell count in the four groups.

	RBC (10^{12}/L)	HB (g/L)	PLT (10^9/L)	WBC (10^9/L)
Control	9.27 ± 0.59	143.6 ± 8.76	554.2 ± 147.65	4.5 ± 0.62
USMB	9.41 ± 0.86	144.8 ± 6.83	519 ± 117.85	4.36 ± 0.41
GO-DOX	8.98 ± 1.12	145.1 ± 11.02	546.4 ± 81.79	4.1 ± 0.58
USMB+GO-DOX	9.14 ± 1.43*	146.4 ± 6.66*	549.6 ± 68.14*	3.88 ± 0.49*

RBC: red blood cell; HB: hemoglobin; PLT: platelet; WBC: white blood cell. *$P > 0.05$ compared with the control, USMB, and GO-DOX groups.

As shown in Figure 9, the RBC in the four groups are biconcave discs with no nucleus, have a diameter of 8 to 10 μm, and have an area of central pallor. The leukocytes are spherical, and the nuclear chromatin is lumpy. The diameter of the WBC is 14 to 20 μm. The nuclei have various shapes, some of which are sausage-like, are rod-like, and have lobulated blue-purple granules. The platelet volume is the smallest, with a diameter of 2 to 4 μm. In blood smears, platelets are usually polygonal and aggregate in groups. Importantly, there were no significant differences in blood cell morphology among the four groups nor were there differences in cell counts, indicating that GO-DOX had no effect on blood cells in nude mice.

3.4.2. Serum Biochemical Tests. The results of the liver and renal functional tests in the four groups are provided in Table 3. There were no significant differences between the USMB+GO-DOX and the control, USMB, and GO-DOX groups in the ALT test, with $t = 0.73$, $P = 0.4813$; $t = 0.97$, $P = 0.3612$; and $t = 0.28$, $P = 0.7672$, respectively. There were no significant differences between the USMB +GO-DOX and the control, USMB, and GO-DOX groups in the AST test, with $t = 1.92$, $P = 0.0904$; $t = 1.27$, $P = 0.2414$; and $t = 0.33$, $P = 0.7528$, respectively. There were no significant differences between the USMB+GO-DOX and the control, USMB, and GO-DOX groups in the CREA test with $t = 2.04$, $P = 0.0758$; $t = 1.57$, $P = 0.1544$; and $t = 1.15$, $P = 0.2818$, respectively. There were no significant differences between the USMB+GO-DOX and the control, USMB, and GO-DOX groups in the BUN test with $t = 1.8$, $P = 0.11$; $t = 0.02$, $P = 0.9841$; and $t = 1.46$, $P = 0.1813$, respectively.

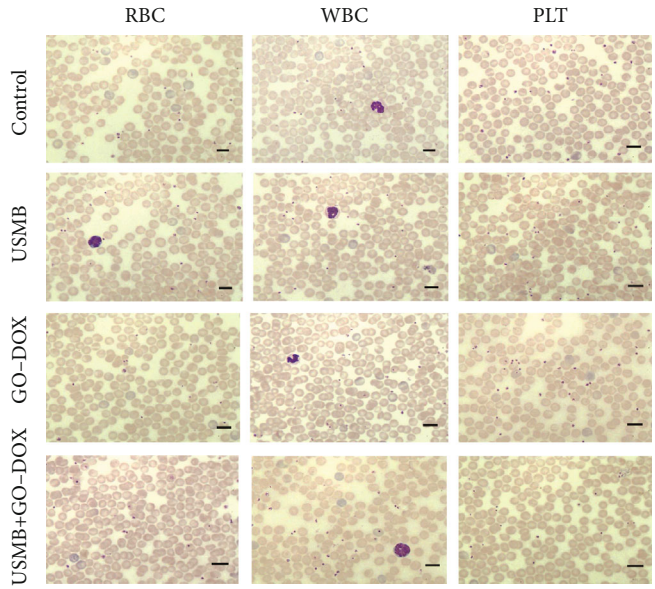

Figure 9: Blood smears after therapy (1000x; bar: 10 μm).

Table 3: Biochemical detection of the liver and kidney function tests in the four groups.

	ALT (U/L)	AST (U/L)	CREA (μmol/L)	BUN (mmol/L)
Control	34 ± 4	173.2 ± 15.99	14.82 ± 1.15	8.73 ± 1.25
USMB	32.4 ± 6.8	182 ± 17.04	14.9 ± 1.84	9.98 ± 1.72
GO-DOX	35 ± 7.7	194.8 ± 21.84	15.41 ± 1.72	10.72 ± 0.69
USMB+GO-DOX	37 ± 8.15*	199.8 ± 26.44*	16.62 ± 1.61*	9.99 ± 0.91*

ALT: alanine transaminase; AST: aspartate transaminase; CREA: creatinine; BUN: blood urea nitrogen. *$P > 0.05$ compared with the control, USMB, and GO-DOX groups.

The results of the liver function (ALT and AST) and kidney function (CREA and BUN) tests showed no significant differences, indicating that GO-DOX is nontoxic to the biochemical detection of nude mice.

3.4.3. HE Staining of the Major Internal Organs. In the four groups, HE staining of cardiac tissue sections showed myocardial cells with myocardial striated fibers and nuclei located in the center of the cardiomyocyte. The structure of hepatocytes showed that these cells were arranged in cords and were polygonal with round nuclei, and central veins were found in some of the histology of liver tissues. The splenic parenchyma consisted of white and red pulps, and the white pulp consisted of dense lymphocytes. Lung cells were seen as hemispherical vesicles composed of monolayer epithelial cells. The kidney biopsy samples contained normal Bowman capsules surrounding glomeruli as well as convoluted tubules (Figure 10).

3.5. Survival Time Follow-Up. Nude mice treated with USMB +GO-DOX had a significantly longer overall survival compared to the control, USMB, and GO-DOX groups ($\chi^2 = 23.44$, $P < 0.0001$) (Figure 11).

4. Discussion

4.1. Effects of USMB+GO-DOX. The results of TEM showed that the tumor microvascular walls of the USMB and USMB+GO-DOX groups were broken and that RBC leaked into the tissue gap (Figure 8).

In the USMB+GO-DOX group, the MBs delivered US energy to sites contiguous with the endothelial cells lining the neovasculature [48], resulting in their disruption, and allowed the GO-DOX to enter the interstitial space of the tumor tissue through the damaged capillaries. The extracellular and intracellular environments of cancer cells have weak acidic conditions [63, 64]. Usually, under low pH conditions, DOX separates from GO [65], entering tumor cells and intercalating with the DNA [66]. The molecular structure of DOX can intercalate into the double strands of DNA of tumor cells forming stable complexes which can affect DNA replication and RNA synthesis [67], inhibit the function of topoisomerase II, promote apoptosis of tumor cells [68] (Figures 6 and 7), decrease proliferation of tumor cells, and prolong the survival time of nude mice. Improving vascular permeability to enhance chemotherapeutic drug uptake yields the potential to improve drug delivery and therapeutic efficacy.

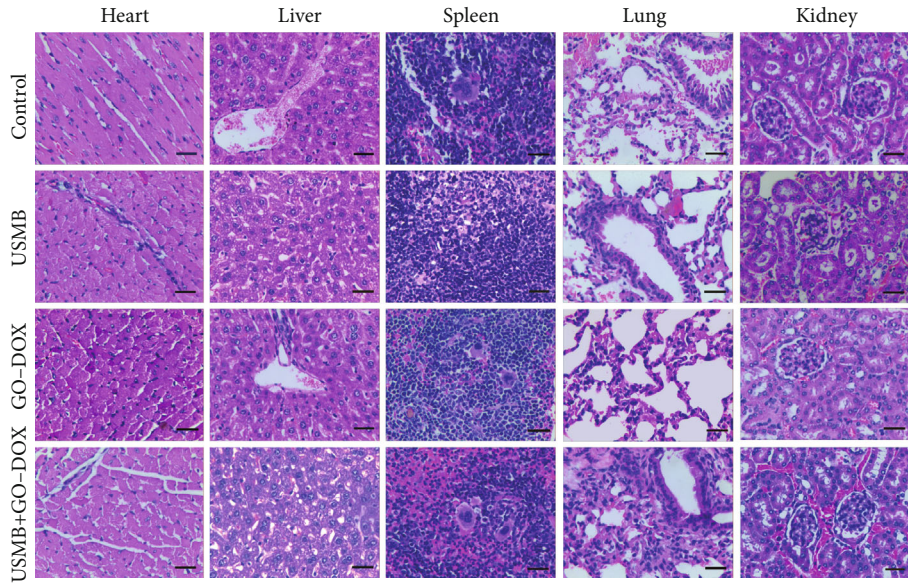

Figure 10: HE staining of the heart, liver, spleen, lung, and kidney after therapy (200x; bar: 50 μm).

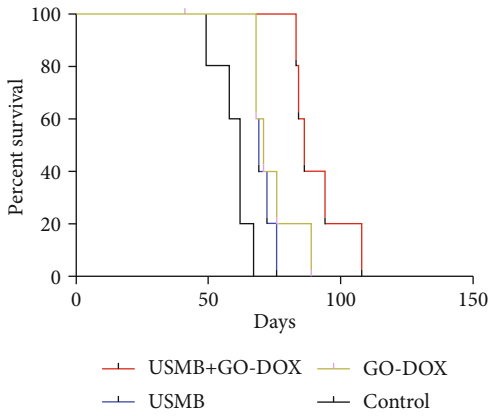

Figure 11: Survival time of the nude mice.

After irradiating the transplanted hepatic carcinoma with 20 kHz US combined with MBs in nude mice, the tail vein was injected with GO-DOX, a chemotherapeutic drug. DOX entered the tumor cells through the broken areas of the damaged vessel walls induced by the cavitation effect, killing these cells by increasing the rate of apoptosis. Indeed, the apoptotic rate of tumor cells in the USMB+GO-DOX group was higher than those in the other three groups (Figure 7). In the GO-DOX group, the blood vessel wall was intact due to the absence of USMB stimulation resulting in a decrease in the amount of chemotherapeutic drug entering the tumor tissue, which resulted in a lower apoptotic rate when compared to the USMB+GO-DOX group. The apoptotic rate was also lower in the USMB group which did not receive chemotherapeutic drugs.

4.2. Benefits of USMB and GO-DOX Combination. The toxicity and side effects of DOX are strong [69]. After DOX is loaded on GO, its toxicity is significantly decreased [70]. In addition, the drug load efficiency of the chemotherapeutic agent is increased [71]. In our experiments, the loading efficiency is 100% (GO concentration 40 μg/mL : DOX concentration 40 μg/mL). Reports show that the gap between tumor capillaries is 100 to 700 nm [72]. However, the diameter of GO-DOX particles is large, and according to our FE-TEM, the diameter of many GO-DOX particles is larger than 1 μm (Figure 5) which hinders their ability to pass directly through the capillary gap of tumors. Therefore, our research was to use low-frequency US combined with MBs to produce a cavitation effect with the goal of damaging blood vessels and destroying the blood vessel wall of tumors, which was demonstrated by TEM (Figure 8). Consequently, GO-DOX would then be able to enter the tumor tissue through the ruptured blood vessels. In an acidic environment, which is present in tumor cells, DOX is released from GO [65] and enters the cell nucleus to promote apoptosis [73]. This method helps GO-DOX penetrate the tumor vascular barrier and enter the tumor tissue. The insonation of a solid tumor with low-frequency US in the presence of an intravascular chemotherapeutic agent can potentiate and localize cytotoxic effects to cancer cells while minimizing side effects in adjacent normal tissue [74].

4.3. Comparisons with Other Related Studies. Low-intensity US (1.0 W/cm^2, 1 MHz, 10% duty factor, 15-minute duration, and without MBs) combined with the chemotherapy agent scutellarin protects nude mice in a xenograft model of human tongue cancer [75]. In the absence of MBs, the mechanism of US-enhanced chemotherapy is not a cavitation effect but a mechanical effect [75]. Theoretically, US can increase the frequency and area of drug-cell contacts, so that the mechanical pressure generated at the contact sites increases the probability of the drug entering cells, enhancing drug absorption and thereby producing a better therapeutic effect [75].

After adding MBs, the mechanism of US-enhanced chemotherapy is mainly a cavitation effect [76]. Cavitation-

enhanced drug absorption depends on the application of MBs [76]. Intravenous epirubicin hydrochloride combined with US (1 MHz) MB therapy *in situ* showed that epirubicin hydrochloride could effectively inhibit the growth of tumors and improve the survival status of mice [76].

Cavitation of MBs enhances the effect of chemotherapy [77]. US (1.011 MHz, 0.064 W/cm^2) irradiation of MBs and melphalan synergistically inhibited *in vivo* malignant melanoma tumor growth [77]. The combination of anticancer drugs and US-MB can inhibit tumor growth even at lower dosages [77].

Compared to studies from Lu et al. [76], Matsuo et al. [77], and Sorace et al. [78], we used a lower US frequency (20 kHz). In principle, the lower the frequency of the sound wave, the longer the expanded phase of sound field and a greater expansion diameter of MBs are produced; in the compressed phase, generating an increased damage effect, a more violent cavitation effect will be produced.

4.4. Toxicity of GO-DOX. The histological results showed that there were no significant abnormalities in the major organs of viscera among the four groups, indicating that GO-DOX had no toxic effect on these organs.

The concentration of DOX in GO-DOX was 0.6 mg/kg in our experiments. Previous studies have shown that 8 mg/kg DOX injected in the tail vein of nude mice can cause death [79]. Lower concentrations, such as 1.33 and 2.67 mg/kg, are not fatal [79], so the usage of our lower concentration could be considered safe. At low (0.1 mg) and medium doses (0.25 mg) of intravenous injection, GO had no obvious toxic side effects on the organs of nude mice [80]. At a higher dose (0.4 mg) of GO in tail vein injections each time in nude mice, chronic side effects, such as pulmonary granuloma, were observed [80]. After 7 days of intravenous injections with the same dose, the nude mice died [80]. In our experiments, GO was used at 12 μg, which lies in the low-dose range. Therefore, the doses of GO we used in nude mice are safe. Histological examination by HE staining disclosed that there were no abnormal cells in the heart, liver, spleen, lung, and kidney of nude mice among the four groups, and there were no differences between the treated groups (Figure 10). Blood test results also showed that there were no adverse effects between the groups (Figure 9). Taken together, the graphene oxide-doxorubicin we used in nude mice was not toxic.

While the subcutaneous tumors of nude mice were irradiated by low-frequency ultrasound, the normal subcutaneous blood vessels were not studied. After injection of microbubbles into the tail vein, they are distributed in the blood vessels of the whole body. The cavitation effect in normal subcutaneous tissues irradiated by low-frequency ultrasound may be inevitable and may have a destructive effect on the blood vessels of normal tissues. This potential side effect should be further studied in the future.

5. Conclusions

In this study, tumor-bearing nude mice were studied. US irradiation combined with a microbubble contrasting agent was used to irradiate the tumor, destroy the blood vessels, and enhance the permeability of a chemotherapeutic agent. This treatment allowed GO-DOX to enter tumor cells through the broken blood vessels and promote apoptosis, prolonging the survival time of the mice and inhibiting tumor growth. Biocompatibility tests of GO-DOX showed that the low dose of GO-DOX (0.6 mg/kg) was safe for *in vivo* applications. Ultrasonic cavitation can enhance the targeted delivery of nanomaterials to tumors of nude mice *in vivo*.

Data Availability

The data used to support the findings of this study are included within the article.

Conflicts of Interest

There are no conflicts to declare.

Authors' Contributions

Zhi Yong Shen and Bei Qi Shen contributed equally to the manuscript.

Acknowledgments

We are grateful to the projects supported by Six Talent Peaks Project in Jiangsu Province (Grant No. 2015-WSW-081), Nantong Health Commission Research project (Grant No. MB2019018), and Nantong University clinical medicine project (2019LY033).

References

[1] M. Ikeda, C. Morizane, M. Ueno, T. Okusaka, H. Ishii, and J. Furuse, "Chemotherapy for hepatocellular carcinoma: current status and future perspectives," *Japanese Journal of Clinical Oncology*, vol. 48, no. 2, pp. 103–114, 2018.

[2] D. Cardinale, A. Colombo, G. Bacchiani et al., "Early detection of anthracycline cardiotoxicity and improvement with heart failure Therapy," *Circulation*, vol. 131, no. 22, pp. 1981–1988, 2015.

[3] F. Chekin, V. Myshin, R. Ye et al., "Graphene-modified electrodes for sensing doxorubicin hydrochloride in human plasma," *Analytical and Bioanalytical Chemistry*, vol. 411, no. 8, pp. 1509–1516, 2019.

[4] M. Baxter-Holland and C. R. Dass, "Doxorubicin, mesenchymal stem cell toxicity and antitumour activity: implications for clinical use," *The Journal of Pharmacy and Pharmacology*, vol. 70, no. 3, pp. 320–327, 2018.

[5] L. P. Swift, S. M. Cutts, A. Nudelman, I. Levovich, A. Rephaeli, and D. R. Phillips, "The cardio-protecting agent and topoisomerase II catalytic inhibitor sobuzoxane enhances doxorubicin-DNA adduct mediated cytotoxicity," *Cancer Chemotherapy and Pharmacology*, vol. 61, no. 5, pp. 739–749, 2008.

[6] E. L. De Beer, A. E. Bottone, and E. E. Voest, "Doxorubicin and mechanical performance of cardiac trabeculae after acute and chronic treatment: a review," *European Journal of Pharmacology*, vol. 415, no. 1, pp. 1–11, 2001.

[7] M. Caru, D. Corbin, D. Périé et al., "Doxorubicin treatments induce significant changes on the cardiac autonomic nervous system in childhood acute lymphoblastic leukemia long-term survivors," *Clinical Research in Cardiology*, vol. 108, no. 9, pp. 1000–1008, 2019.

[8] A. A. Kirkham, N. D. Eves, R. E. Shave et al., "The effect of an aerobic exercise bout 24 h prior to each doxorubicin treatment for breast cancer on markers of cardiotoxicity and treatment symptoms: a RCT," *Breast Cancer Research and Treatment*, vol. 167, no. 3, pp. 719–729, 2018.

[9] E. Calvo, V. Moreno, M. Flynn et al., "Antitumor activity of lurbinectedin (PM01183) and doxorubicin in relapsed small-cell lung cancer: results from a phase I study," *Annals of Oncology*, vol. 28, no. 10, pp. 2559–2566, 2017.

[10] K. T. Brown, R. K. Do, M. Gonen et al., "Randomized trial of hepatic artery embolization for hepatocellular carcinoma using doxorubicin-eluting microspheres compared with embolization with microspheres alone," *Journal of Clinical Oncology*, vol. 34, no. 17, pp. 2046–2053, 2016.

[11] W. M. Sikov, D. A. Berry, C. M. Perou et al., "Impact of the addition of carboplatin and/or bevacizumab to neoadjuvant once-per-week paclitaxel followed by dose-dense doxorubicin and cyclophosphamide on pathologic complete response rates in stage II to III triple-negative breast cancer: CALGB 40603 (Alliance)," *Journal of Clinical Oncology*, vol. 33, no. 1, pp. 13–21, 2015.

[12] J. C. Dean, S. E. Salmon, and K. S. Griffith, "Prevention of doxorubicin-induced hair loss with scalp hypothermia," *The New England Journal of Medicine*, vol. 301, no. 26, pp. 1427–1429, 1979.

[13] P. Vejpongsa and E. T. H. Yeh, "Prevention of Anthracycline-Induced Cardiotoxicity: Challenges and Opportunities," *Journal of the American College of Cardiology*, vol. 64, no. 9, pp. 938–945, 2014.

[14] K. Renu, V. G. Abilash, P. B. Tirupathi Pichiah, and S. Arunachalam, "Molecular mechanism of doxorubicin-induced cardiomyopathy - an update," *European Journal of Pharmacology*, vol. 818, pp. 241–253, 2018.

[15] L. Zhang, X. Qu, Y. Teng et al., "Efficacy of thalidomide in preventing delayed nausea and vomiting induced by highly emetogenic chemotherapy: a randomized, multicenter, double-blind, placebo-controlled phase III trial (CLOG1302 study)," *Journal of Clinical Oncology*, vol. 35, no. 31, pp. 3558–3565, 2017.

[16] I. Vargel, A. Erdem, D. Ertoy et al., "Effects of growth factors on doxorubicin-induced skin necrosis: documentation of histomorphological alterations and early treatment by GM-CSF and G-CSF," *Annals of Plastic Surgery*, vol. 49, no. 6, pp. 646–653, 2002.

[17] Y. Liu, L. Qiao, S. Zhang et al., "Dual pH-responsive multifunctional nanoparticles for targeted treatment of breast cancer by combining immunotherapy and chemotherapy," *Acta Biomaterialia*, vol. 66, pp. 310–324, 2018.

[18] R. Yekani, E. Rusak, A. Riaz et al., "Formation of nanocrystalline graphene on germanium," *Nanoscale*, vol. 10, no. 25, pp. 12156–12162, 2018.

[19] X. Huang, Z. Zeng, Z. Fan, J. Liu, and H. Zhang, "Graphene-based electrodes," *Advanced Materials*, vol. 24, no. 45, pp. 5979–6004, 2012.

[20] X. Zhou and F. Liang, "Application of graphene/graphene oxide in biomedicine and biotechnology," *Current Medicinal Chemistry*, vol. 21, no. 7, pp. 855–869, 2014.

[21] J. Kim, S. J. Park, and D. H. Min, "Emerging approaches for graphene oxide biosensor," *Analytical Chemistry*, vol. 89, no. 1, pp. 232–248, 2016.

[22] G. Shim, M. G. Kim, J. Y. Park, and Y. K. Oh, "Graphene-based nanosheets for delivery of chemotherapeutics and biological drugs," *Advanced Drug Delivery Reviews*, vol. 105, pp. 205–227, 2016.

[23] I. Ocsoy, N. Isiklan, S. Cansiz, N. Özdemir, and W. Tan, "ICG-conjugated magnetic graphene oxide for dual photothermal and photodynamic therapy," *RSC Advances*, vol. 6, no. 36, pp. 30285–30292, 2016.

[24] R. Justin and B. Chen, "Characterisation and drug release performance of biodegradable chitosan-graphene oxide nanocomposites," *Carbohydrate Polymers*, vol. 103, pp. 70–80, 2014.

[25] H. P. Cong, J. F. Chen, and S. H. Yu, "Graphene-based macroscopic assemblies and architectures: an emerging material system," *Chemical Society Reviews*, vol. 43, no. 21, pp. 7295–7325, 2014.

[26] A. Bonanni, C. K. Chua, and M. Pumera, "Rational design of carboxyl groups perpendicularly attached to a graphene sheet: a platform for enhanced biosensing applications," *Chemistry*, vol. 20, no. 1, pp. 217–222, 2014.

[27] V. V. Neklyudov, N. R. Khafizov, I. A. Sedov, and A. M. Dimiev, "New insights into the solubility of graphene oxide in water and alcohols," *Physical Chemistry Chemical Physics*, vol. 19, no. 26, pp. 17000–17008, 2017.

[28] S. M. Mousavi, S. A. Hashemi, Y. Ghasemi, A. M. Amani, A. Babapoor, and O. Arjmand, "Applications of graphene oxide in case of nanomedicines and nanocarriers for biomolecules: review study," *Drug Metabolism Reviews*, vol. 51, no. 1, pp. 12–41, 2019.

[29] C. Huang, X. Hu, Z. Hou, J. Ji, Z. Li, and Y. Luan, "Tailored graphene oxide-doxorubicin nanovehicles via near-infrared dye-lactobionic acid conjugates for chemo-photothermal therapy," *Journal of Colloid and Interface Science*, vol. 545, pp. 172–183, 2019.

[30] B. Zhang, X. Yang, Y. Wang, and G. Zhai, "Heparin modified graphene oxide for pH-sensitive sustained release of doxorubicin hydrochloride," *Materials Science & Engineering: C Materials for Biological Applications*, vol. 75, pp. 198–206, 2017.

[31] M. Mahdavi, F. Rahmani, and S. Nouranian, "Molecular simulation of pH-dependent diffusion, loading, and release of doxorubicin in graphene and graphene oxide drug delivery systems," *Journal of Materials Chemistry B*, vol. 4, no. 46, pp. 7441–7451, 2016.

[32] W. Zhou, M. Y. Fong, Y. Min et al., "Cancer-secreted miR-105 destroys vascular endothelial barriers to promote metastasis," *Cancer Cell*, vol. 25, no. 4, pp. 501–515, 2014.

[33] D. K. Kirui, E. J. Koay, X. Guo, V. Cristini, H. Shen, and M. Ferrari, "Tumor vascular permeabilization using localized mild hyperthermia to improve macromolecule transport," *Nanomedicine*, vol. 10, no. 7, pp. 1487–1496, 2014.

[34] B. Zhang, T. Jiang, Y. Tuo et al., "Captopril improves tumor nanomedicine delivery by increasing tumor blood perfusion and enlarging endothelial gaps in tumor blood vessels," *Cancer Letters*, vol. 410, pp. 12–19, 2017.

[35] O. Ngo, E. Niemann, V. Gunasekaran et al., "Development of low frequency (20-100 kHz) clinically viable ultrasound applicator for chronic wound treatment," *IEEE Transactions on*

Ultrasonics, Ferroelectrics, and Frequency Control, vol. 66, no. 3, pp. 572–580, 2019.

[36] A. Bubulis, V. Garalienė, V. Jurėnas, J. Navickas, and S. Giedraitis, "Effect of low-intensity cavitation on the isolated human thoracic artery *in vitro*," *Ultrasound in Medicine & Biology*, vol. 43, no. 5, pp. 1040–1047, 2017.

[37] I. Tzanakis, G. S. B. Lebon, D. G. Eskin, and K. A. Pericleous, "Characterizing the cavitation development and acoustic spectrum in various liquids," *Ultrasonics Sonochemistry*, vol. 34, pp. 651–662, 2017.

[38] K. Nakajima, D. Nishioka, M. Hirao, M. So, Y. Goto, and H. Ogi, "Drastic acceleration of fibrillation of insulin by transient cavitation bubble," *Ultrasonics Sonochemistry*, vol. 36, pp. 206–211, 2017.

[39] F. Ahmadi, I. V. McLoughlin, S. Chauhan, and G. ter-Haar, "Bio-effects and safety of low-intensity, low-frequency ultrasonic exposure," *Progress in Biophysics and Molecular Biology*, vol. 108, no. 3, pp. 119–138, 2012.

[40] R. R. Sun, M. L. Noble, S. S. Sun, S. Song, and C. H. Miao, "Development of therapeutic microbubbles for enhancing ultrasound-mediated gene delivery," *Journal of Controlled Release*, vol. 182, pp. 111–120, 2014.

[41] S. Bhatnagar, J. J. Kwan, A. R. Shah, C. C. Coussios, and R. C. Carlisle, "Exploitation of sub-micron cavitation nuclei to enhance ultrasound-mediated transdermal transport and penetration of vaccines," *Journal of Controlled Release*, vol. 238, pp. 22–30, 2016.

[42] S. V. Sancheti and P. R. Gogate, "A review of engineering aspects of intensification of chemical synthesis using ultrasound," *Ultrasonics Sonochemistry*, vol. 36, pp. 527–543, 2017.

[43] N. V. Dezhkunov, A. Francescutto, L. Serpe, R. Canaparo, and G. Cravotto, "Sonoluminescence and acoustic emission spectra at different stages of cavitation zone development," *Ultrasonics Sonochemistry*, vol. 40, pp. 104–109, 2018.

[44] Z. Y. Shen, G. L. Xia, M. F. Wu, L. Y. Ji, and Y. J. Li, "The effects of percutaneous ethanol injection followed by 20-kHz ultrasound and microbubbles on rabbit hepatic tumors," *Journal of Cancer Research and Clinical Oncology*, vol. 142, no. 2, pp. 373–378, 2016.

[45] Z. Y. Shen, G. L. Xia, M. F. Wu et al., "The effects of low-frequency ultrasound and microbubbles on rabbit hepatic tumors," *Experimental Biology and Medicine*, vol. 239, no. 6, pp. 747–757, 2014.

[46] H. Hashemi and H. Namazi, "Sonochemically synthesized blue fluorescent functionalized graphene oxide as a drug delivery system," *Ultrasonics Sonochemistry*, vol. 42, pp. 124–133, 2018.

[47] K. Ryu, J. Park, and T. I. Kim, "Effect of pH-responsive charge-conversional polymer coating to cationic reduced graphene oxide nanostructures for tumor microenvironment-targeted drug delivery systems," *Nanomaterials*, vol. 9, no. 9, p. 1289, 2019.

[48] M. W. Cheng, F. Li, T. Han, A. C. H. Yu, and P. Qin, "Effects of ultrasound pulse parameters on cavitation properties of flowing microbubbles under physiologically relevant conditions," *Ultrasonics Sonochemistry*, vol. 52, pp. 512–521, 2019.

[49] L. Y. Wang and S. S. Zheng, "Advances in low-frequency ultrasound combined with microbubbles in targeted tumor therapy," *Journal of Zhejiang University-Science B*, vol. 20, no. 4, pp. 291–299, 2019.

[50] W. Cheng-Hui, M. Run-Yang, and H. Jing, "Acoustic response of bubbles inside a cylindrical cavitationbubble cluster generated by low-frequency ultrasound," *Acta Physica Sinica*, vol. 65, no. 14, pp. 149–156, 2016.

[51] J. L. Hardcastle, J. C. Ball, Q. Hong et al., "Sonoelectrochemical and sonochemical effects of cavitation: correlation with interfacial cavitation induced by 20 kHz ultrasound," *Ultrasonics Sonochemistry*, vol. 7, no. 1, pp. 7–14, 2000.

[52] A. Amiri, P. Sharifian, and N. Soltanizadeh, "Application of ultrasound treatment for improving the physicochemical, functional and rheological properties of myofibrillar proteins," *International Journal of Biological Macromolecules*, vol. 111, pp. 139–147, 2018.

[53] E. Hapeshi, A. Achilleos, A. Papaioannou et al., "Sonochemical degradation of ofloxacin in aqueous solutions," *Water Science and Technology*, vol. 61, no. 12, pp. 3141–3146, 2010.

[54] N. Porova, V. Botvinnikova, O. Krasulya, P. Cherepanov, and I. Potoroko, "Effect of ultrasonic treatment on heavy metal decontamination in milk," *Ultrasonics Sonochemistry*, vol. 21, no. 6, pp. 2107–2111, 2014.

[55] G. A. Husseini, G. D. Myrup, W. G. Pitt, D. A. Christensen, and N. Y. Rapoport, "Factors affecting acoustically triggered release of drugs from polymeric micelles," *Journal of Controlled Release*, vol. 69, no. 1, pp. 43–52, 2000.

[56] H. Yang, Z. H. Liu, Y. Y. Liu, C. C. Lou, Z. L. Ren, and H. Miyoshi, "Vascular gene transfer and drug delivery in vitro using low-frequency ultrasound and microbubbles," *Acta Pharmacologica Sinica*, vol. 31, no. 4, pp. 515–522, 2010.

[57] H. Liu, H. W. Xu, Y. Z. Zhang et al., "Ursodeoxycholic acid induces apoptosis in hepatocellular carcinoma xenografts in mice," *World Journal of Gastroenterology*, vol. 21, no. 36, pp. 10367–10374, 2015.

[58] K. Yang, H. Gong, X. Shi, J. Wan, Y. Zhang, and Z. Liu, "In vivo biodistribution and toxicology of functionalized nanographene oxide in mice after oral and intraperitoneal administration," *Biomaterials*, vol. 34, no. 11, pp. 2787–2795, 2013.

[59] A. Deb, N. G. Andrews, and V. Raghavan, "Natural polymer functionalized graphene oxide for co-delivery of anticancer drugs: in-vitro and in-vivo," *International Journal of Biological Macromolecules*, vol. 113, pp. 515–525, 2018.

[60] M. Amrollahi-Sharifabadi, M. K. Koohi, E. Zayerzadeh, M. H. Hablolvarid, J. Hassan, and A. M. Seifalian, "In vivo toxicological evaluation of graphene oxide nanoplatelets for clinical application," *International Journal of Nanomedicine*, vol. - Volume 13, pp. 4757–4769, 2018.

[61] M. C. Duch, G. R. S. Budinger, Y. T. Liang et al., "Minimizing oxidation and stable nanoscale dispersion improves the biocompatibility of graphene in the lung," *Nano Letters*, vol. 11, no. 12, pp. 5201–5207, 2011.

[62] M. Zheng, W. Zheng, W. Wang et al., "Study on the effect of ginsenosides Rb on blood of tumor mice," *BioMed Research International*, vol. 2019, Article ID 5476076, 6 pages, 2019.

[63] J. Song, Z. Ge, X. Yang et al., "Hepatic stellate cells activated by acidic tumor microenvironment promote the metastasis of hepatocellular carcinoma via osteopontin," *Cancer Letters*, vol. 356, no. 2, pp. 713–720, 2015.

[64] C. R. Justus, L. Dong, and L. V. Yang, "Acidic tumor microenvironment and pH-sensing G protein-coupled receptors," *Frontiers in Physiology*, vol. 4, p. 354, 2013.

[65] E. Song, W. Han, C. Li et al., "Hyaluronic acid-decorated graphene oxide nanohybrids as nanocarriers for targeted and pH-responsive anticancer drug delivery," *ACS Applied Materials & Interfaces*, vol. 6, no. 15, pp. 11882–11890, 2014.

[66] Y. T. Fong, C.-H. Chen, and J.-P. Chen, "Intratumoral delivery of doxorubicin on folate-conjugated graphene oxide by in-situ forming thermo-sensitive hydrogel for breast cancer therapy," *Nanomaterials*, vol. 7, no. 11, p. 388, 2017.

[67] J. Cox and S. Weinman, "Mechanisms of doxorubicin resistance in hepatocellular carcinoma," *Hepatic Oncology*, vol. 3, no. 1, pp. 57–59, 2016.

[68] H. Li, Y. Cui, J. Sui et al., "Efficient delivery of DOX to nuclei of hepatic carcinoma cells in the subcutaneous tumor model using pH-sensitive pullulan-DOX conjugates," *ACS Applied Materials & Interfaces*, vol. 7, no. 29, pp. 15855–15865, 2015.

[69] A. Shafei, W. el-Bakly, A. Sobhy et al., "A review on the efficacy and toxicity of different doxorubicin nanoparticles for targeted therapy in metastatic breast cancer," *Biomedicine & Pharmacotherapy*, vol. 95, pp. 1209–1218, 2017.

[70] M. Hashemi, A. Yadegari, G. Yazdanpanah et al., "Normalization of doxorubicin release from graphene oxide: new approach for optimization of effective parameters on drug loading," *Biotechnology and Applied Biochemistry*, vol. 64, no. 3, pp. 433–442, 2017.

[71] Y. Lv, L. Tao, S. W. Annie Bligh, H. Yang, Q. Pan, and L. Zhu, "Targeted delivery and controlled release of doxorubicin into cancer cells using a multifunctional graphene oxide," *Materials Science & Engineering: C Materials for Biological Applications*, vol. 59, pp. 652–660, 2016.

[72] W. Luo, G. Wen, L. Yang et al., "Dual-targeted and pH-sensitive doxorubicin prodrug-microbubble complex with ultrasound for tumor treatment," *Theranostics*, vol. 7, no. 2, pp. 452–465, 2017.

[73] M. Singh, P. Gupta, R. Baronia et al., "In vitro cytotoxicity of GO-DOx on FaDu squamous carcinoma cell lines," *International Journal of Nanomedicine*, vol. 13, pp. 107–111, 2018.

[74] A. K. W. Wood and C. M. Sehgal, "A review of low-intensity ultrasound for cancer therapy," *Ultrasound in Medicine & Biology*, vol. 41, no. 4, pp. 905–928, 2015.

[75] H. Li, H. Fan, Z. Wang, J. Zheng, and W. Cao, "Potentiation of scutellarin on human tongue carcinoma xenograft by low-intensity ultrasound," *PLoS One*, vol. 8, no. 3, article e59473, 2013.

[76] C. T. Lu, Y. Z. Zhao, Y. Wu et al., "Experiment on enhancing antitumor effect of intravenous epirubicin hydrochloride by acoustic cavitation in situ combined with phospholipid-based microbubbles," *Cancer Chemotherapy and Pharmacology*, vol. 68, no. 2, pp. 343–348, 2011.

[77] M. Matsuo, K. Yamaguchi, L. B. Feril Jr. et al., "Synergistic inhibition of malignant melanoma proliferation by melphalan combined with ultrasound and microbubbles," *Ultrasonics Sonochemistry*, vol. 18, no. 5, pp. 1218–1224, 2011.

[78] A. G. Sorace, J. M. Warram, H. Umphrey, and K. Hoyt, "Microbubble-mediated ultrasonic techniques for improved chemotherapeutic delivery in cancer," *Journal of Drug Targeting*, vol. 20, no. 1, pp. 43–54, 2011.

[79] J. L. Nelson, B. L. Roeder, J. C. Carmen, F. Roloff, and W. G. Pitt, "Ultrasonically activated chemotherapeutic drug delivery in a rat model," *Cancer Research*, vol. 62, no. 24, pp. 7280–7283, 2002.

[80] S. F. Kiew, L. V. Kiew, H. B. Lee, T. Imae, and L. Y. Chung, "Assessing biocompatibility of graphene oxide-based nanocarriers: a review," *Journal of Controlled Release*, vol. 226, pp. 217–228, 2016.